

PCCP

Physical Chemistry Chemical Physics

Accepted Manuscript

This article can be cited before page numbers have been issued, to do this please use: H. Abdelsalam, W. Othman, V. Saroka, N. Teleb, S. Yunoki and Q. Zhang, *Phys. Chem. Chem. Phys.*, 2020, DOI: 10.1039/C9CP06823F.



This is an Accepted Manuscript, which has been through the Royal Society of Chemistry peer review process and has been accepted for publication.

Accepted Manuscripts are published online shortly after acceptance, before technical editing, formatting and proof reading. Using this free service, authors can make their results available to the community, in citable form, before we publish the edited article. We will replace this Accepted Manuscript with the edited and formatted Advance Article as soon as it is available.

You can find more information about Accepted Manuscripts in the [Information for Authors](#).

Please note that technical editing may introduce minor changes to the text and/or graphics, which may alter content. The journal's standard [Terms & Conditions](#) and the [Ethical guidelines](#) still apply. In no event shall the Royal Society of Chemistry be held responsible for any errors or omissions in this Accepted Manuscript or any consequences arising from the use of any information it contains.

Interaction of hydrated metals with chemically modified hexagonal boron nitride quantum dots: wastewater treatment and water splitting

H. Abdelsalam^{1,2}, W. O. Younis³, V. A. Saroka^{4,5}, N. H. Teleb⁶, S. Yunoki⁷, Q. Zhang^{1*}

¹School of Materials Science and Engineering, Yancheng Institute of Technology, Yancheng 224051, P. R. China.

²Theoretical Physics Department, National Research Centre, El-Buhouth Str., Dokki, Giza, 12622, Egypt.

³Vice Presidency for Postgraduate Studies and Scientific Research, Imam Abdulrahman Bin Faisal University, P.O. Box 1982, Dammam, 31441, Saudi Arabia.

⁴Institute for Nuclear Problems, Belarusian State University, Bobruiskaya 11, 220030 Minsk, Belarus.

⁵Center for Quantum Spintronics, Department of Physics, Norwegian University of Science and Technology, NO-7491 Trondheim, Norway.

⁶Electron Microscope and Thin Films Department, National Research Centre, El-Buhouth Str., Dokki, Giza, 12622, Egypt.

⁷Computational Condensed Matter Physics Laboratory, RIKEN, Wako, Saitama 351-0198, Japan.

Abstract

The electronic and adsorption properties of chemically modified square hexagonal boron nitride quantum dots are investigated using density functional theory calculations. The free energy and frequency calculations show that all the boron nitride flakes are stable before/after modification and metal adsorption. Edge modification significantly enhances the stability and interactivity of the flake. For instance, the free energy of binding decreases from -6.5 eV in hydrogenated flake to -7.1 eV in pristine one and dipole moment increases from 4.5 D to 54.9 D, respectively. A wide spectrum of band gaps can also be achieved, where the band gap can be smoothly varied from ~ 6 eV in edge fluorinated flakes to 0.2 in sulfured ones. Six hydrated metals, Cd, Co, Cr, Cu, Fe, and Zn, are considered for adsorption by the flakes. The transition metals are highly selected by the flakes while heavy metals are weakly adsorbed. All hydrated metals are physically adsorbed by the edge and surface of hydrogenated flakes except Cu which is chemically adsorbed. Chemical groups or elements attached to the flake strongly enhance the adsorption strength; the adsorption energy of hydrated Cr on surface increases from 0.6 eV to 8.6 eV after attaching two COOH groups to the surface. Hydrogen evolution has also been observed through the adsorption process. The calculated low overpotential for the oxygen evolution reaction (0.52 V) and hydrogen adsorption strength (0.11 eV) for the hydrogen evolution reaction indicate that boron nitride quantum dots are not only potential candidates for the removal of different metals from wastewater but also for efficient water splitting.

1. Introduction

The monolayer of hexagonal boron nitride (hBN) is a two dimensional material called 'white graphene'. It combines properties of graphene and diamond. Similar to graphene, hBN has a bipartite lattice formed by sp² hybridized atoms [1]. However, the two nonequivalent sites of the bipartite lattice host different atomic elements – boron and nitrogen. As a result, hBN has a wide bandgap of about ~5.5 eV that is close to the band gap of diamond [2]. Having very close lattice constant with graphene [3], hBN is considered as promising substrate material for graphene electronics [4–6]. On the other hand, the similarity with diamond makes hBN useful for optoelectronics and integrated quantum photonics: room temperature single photon emitters [7,8], tunable photonic crystal cavities [9,10] and deep subwavelength manipulation of infrared light [11–15].

Similar to graphene hBN can form nanotubes [16,17], nanoribbons [18–21] and quantum dots [22–29]. A variety of hybrid/hetero structures of hBN with graphene have been demonstrated experimentally too [30–36]. The structural, electronic, magnetic, and optical properties of hBN nanotubes [37–46] and nanoribbons [46–52] have been a subject of investigation in semiempirical and first principles studies. Intensive studies have been also undertaken by theorists to reveal and understand the properties of hBN/graphene hetero/hybrid structures [53–60]. However, the hBN quantum dots have been hardly investigated, especially in comparison with the graphene and other 2D material based quantum dots (for instance Refs. [61–77] etc.). Nevertheless, some studies on structural stability, magnetic, optical and adsorption properties can be found in the literature.

The study of the structural stability of the hBN quantum dots showed that a counterintuitive triangular shape of larger perimeter is the equilibrium shape for hBN nanoparticles with zigzag edges, though for some specific chemical conditions a more compact hexagonal shape with armchair edge dominates [78]. A recent theoretical study by Zhang et al. [79] shows that the edges passivated with H atoms are more stable and regular than bare ones, whereas NH-terminated zigzag edges are more stable than H attached armchair edges which in turn more stable than BH-terminated zigzag edges. At the same time, bare armchair edges may be more energetically favorable than N- or B-terminated zigzag edges.

In 2009 Du et al. reported giant magnetic moments, associated spin splitting and half metallicity for triangular hBN quantum dots with NH-terminations [80]. However, Xi et al. reported that for triangular hBN dots the edge passivation removes spin polarization of the ground state. According to this study, in contrast to graphene quantum dots with zigzag edges and triangular shape, the Lieb's theorem is not satisfied in hBN triangular quantum dots with zigzag edges [81]. Xu et al. investigated triangular hBN quantum dot embedded into armchair graphene nanoribbon and graphene in a periodic manner. This study shows that embedment of hBN quantum dots can result in spin-polarized ground states originating from the graphene-hBN interface [82]. In contrast to Xu and co-workers, Xi et al. [83] explored doping of triangular hBN quantum dot with one and two C atoms. Their results show that single C doping always leads to half metallicity and spin polarized states. Similar results have been reported by Yamijala [84,85] although in his case the hBN quantum dots have rectangular and cross-like shapes while the substitutional doping with C covers a significant fraction of the dot edge or interior. Thus, in principle in combination with carbon hBN may be useful for spintronic applications.

Hexagonal boron nitride quantum dots have also been proposed for thermoelectric and gas sensing applications. Pan et al. [86] considered thermoelectric properties of hBN dots at room and low temperatures. In this study, it is shown that the hBN quantum dots have high thermoelectric figure of merit $ZT \sim 0.78(0.95)$ which outperforms that of similar graphene structures. In another study by Neek-Amal and colleagues [87] triaxial strain of about 10% was applied to the N(B) atoms of a hexagonal flake of hBN. This strain localized the lowest unoccupied molecular orbital (LUMO) and highest occupied molecular orbital (HOMO) at the center of the flake making it a perfect gas sensor, for instance for NH_3 molecule. Bandyopadhyay et al. [88] studied physisorption of tetracyanoquinodimethane and tetrathiafulvalene molecules on the surface of rectangular hBN quantum dots. As follows from their results the physisorption introduces new energy states inside the pristine energy gap decreasing HOMO-LUMO gap by half and red-shifting the optical absorption edge below 2 eV. First principle calculations also show facile adsorption of gas molecules (H_2 , CO, NO, O_3 , H_2O , and O_2) and metal oxides (CuO, AgO, AuO) on the surface of H passivated hBN rectangular quantum dot [89]. The effect of adsorption of OLi_4 , NLi_5 , CLi_6 , BLi_7 and Al_2Be metal compounds on monolayer hBN rectangular quantum dots has been analyzed in Ref. [90]. The results of these first principles calculations show that in general adsorption of the above mentioned metal compounds reduces the energy gap of the pristine hBN dot and correspondingly extends the absorption from ultraviolet and visible to infrared frequency range. The hydroxylation of the armchair edge of the rectangular quantum dots of hBN also leads to 20-30% drop in the energy gap. The energy gap of both the hydrogenated and partially hydroxylated hBN rectangular dots can be narrowed by in-plane electric field [91]. The reviewed works indeed suggest that adsorption of the variety of chemical compounds on hBN quantum dots significantly alter their properties which should be useful in sensing applications.

Boron nitride based materials have demonstrated a great potential in wastewater treatment. Recently, it has been reported by Xue et al. [92] that boron nitride porous monoliths demonstrate an excellent adsorption capacity of various oil contaminants in water (up to 71–98% for volume based adsorption capacity). Moreover, these monoliths exhibit ultrahigh removal capacity of rhodamine B (554 mg/g) and Cd(II) (561 mg/g) pollutants. This experimental achievement inspired us to systematically study the hBN quantum dots potential (including size and edge effects) for the water purification and splitting. Our paper is organized as follows: in Section 2 we briefly introduce the computational model, in Section 3 we present the main results on chosen hBN quantum dots structure stability, electronic and adsorption properties, finally in Section 4 we summarize our conclusions. We relegate supplementary results into Appendices.

2. Computational model

In this paper, we study the electronic and adsorption properties of chemically modified square hexagonal boron nitride quantum dots (shBN) using DFT calculations as implemented in Gaussian 16 [93]. The basis set 3-21g* is used in calculations that proved to be adequate when considering both the computational power and the results accuracy [94-96]. The Becke-three parameters-Lee-Yang-Parr hybrid functional (B3LYP) [97,98] is used in our calculations due to the good representation that it shows for shBNs and similar systems, e.g. C-based clusters [99-101]. We also performed additional calculations with different basis sets and functionals to verify the adequacy of the B3LYP/3-21G* level. As shown in Fig. 6 a, Appendix A, the calculated band gap at 3-21g* and higher 6-31g(d,p) and 6-311g(d,p) basis sets have comparable values. For instance, $\Delta E = 4.86$ eV for shBN-OH-S using 3-21g* and 4.83 eV using 6-31g(d,p) while the computational time is twice shorter for the former. The functional B3LYB gives intermediate values of ΔE between that from PBE and Cam-b3lyb. We can say that the B3LYB provides the best description of the band structure because for the large shBN with $n_t=456$, it gives $\Delta E \sim 5.45$ eV which is comparable to that of periodic hBN sheet [2]. While for the same n_t , PBE underestimate the band gap, $\Delta E \sim 3.67$ eV and CAM-B3LYB overestimate it with $\Delta E \sim 8.42$ eV.

3. Results and discussion

In the present work, the electronic and adsorption properties of shBN are studied. The effect of chemical modification of the edge and surface by attaching different elements, namely H, F, O, and S, and chemical groups (COOH, OH, SOH, POH₂) is included and investigated as a tool that tunes the electronic properties and enhances the adsorption process. The hydrogenated flakes are taken as the reference to which we compare change in the electronic properties caused by attaching other elements, groups, and adsorption of hydrated metals.

3.1 Structures Stability

The optimized structures of edge functionalized shBN with various elements and groups are presented in Fig.1. From the figure it can be seen that the square shape of the QDs is retained with small deformation after passivation with H and F elements, and with chemical groups (see Fig. 1 (a), (b), (f)-(i)). While passivation with O, pristine, and S (Fig. 1 (c), (d)) results in a noticeable deformation.

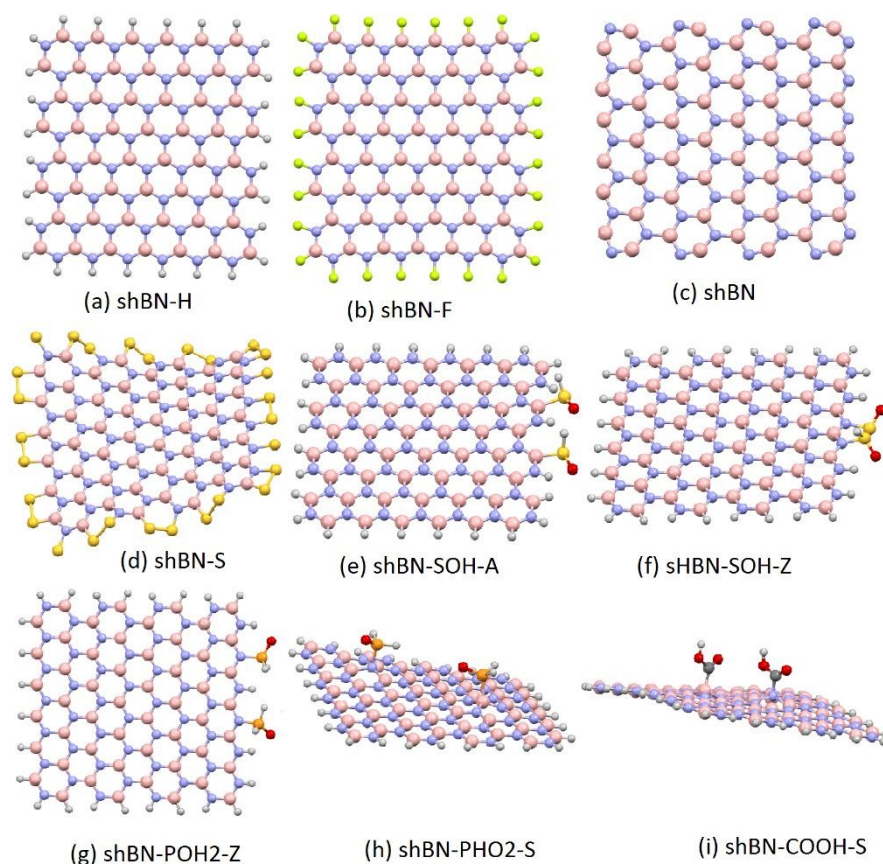


Fig. 1. The structure of chemically modified shBN by different elements and groups. Colored spheres represent B (pink), N (blue), H (silver), F (greenish), S (yellow), O (red), P (orange), and C (gray) atoms.

The B-N bond lengths (d_{BN}) for the edge and surface modified shBN are given in Table 1. The values show that d_{BN} ranges from 1.43 to 1.47 Å in the hydrogenated cluster (shBN-H) where the lower values appear at the armchair edges, the medium at the zigzag edges, and the large ones in the bulk. Similar values can be observed also in fluorinated flakes; these values are comparable to $d_{\text{BN}} = 1.45$ Å in the infinite bulk system [102]. Attachment of chemical groups is considered for three cases, (a) attachment to the armchair edge, (b) to zigzag edge, and (c) to the surface. The B-N bond lengths increase around the attached groups especially in surface adsorption, for example in surface attachment of OH (shBN-OH-S as in Table 1) $d_{\text{BN}}=1.58$ Å, while in other positions it is almost the same like shBN-H. The bond length between the attached element or group (d_x , x refers to the element or the group) are also presented in Table 1. d_x has a wide range of values starting from 1.02 to 3.34 Å depending on the attached element, attachment to B or N in the flake, and the type of the formed bond (chemical/physical). The smallest $d_x=1.02$ Å between

the attached H and the flake N atom, this value increases to 1.20 Å when H is attached to B atom due to the low electronegativity of B (~2.28) with respect to N (~3.19). Increasing the atomic radius of the attached element increases the bond length, as for F, O and S atom in Table 1. The higher bond lengths observed in surface functionalization, from $d_x=1.57$ Å in shBN-OH-S to 3.34 Å in shBN-SOH-S (Table 1), imply that these groups form weaker bonds with the surface.

Table 1. Bond length between B and N atoms (d_{BN}), passivating element and flake (d_x). Free energy of binding (ΔG), energy gap (ΔE), and total electric dipole moment (TEDM).

shBN	d_{BN} (Å)	d_x (Å)	ΔG (eV)	ΔE (eV)	TEDM (D)
shBN-H	1.43-1.47	1.02, 1.20	-6.48	5.59	4.67
shBN-F	1.43-1.48	1.34-1.45	-6.52	6.05	1.29
shBN-O	1.45-1.63	1.23-1.43	-7.03	0.99	4.74
shBN-S	1.42-1.48	1.75,1.85	-6.73	0.16	5.09
shBN	1.35-1.59	---	-7.09	0.18	54.98
shBN-OH-A	1.43-1.47	1.48, 1.38	-6.37	5.08	5.99
shBN-OH-Z	1.43-1.47	1.49	-6.37	5.21	2.61
shBN-OH-S	1.44-1.58	1.48,1.57	-6.29	4.86	9.28
shBN-POH2-A	1.42-1.47	1.96	-6.18	5.55	12.21
shBN-POH2-Z	1.43-1.49	1.70	-6.19	5.89	4.21
shBN-POH2-S	1.43-1.58	1.85, 2.01	-6.09	2.12	28.35
shBN-SOH-A	1.41-1.47	1.94	-6.25	5.22	12.14
shBN-SOH-Z	1.43-1.47	1.73	-6.25	5.73	2.96
shBN-SOH-S	1.43-1.47	3.34, 3.11	-6.19	3.59	4.42
shBN-COOH-A	1.42-1.49	1.61	-6.19	4.51	2.05
shBN-COOH-Z	1.43-1.50	1.34	-6.19	5.68	1.22
shBN-COOH-S	1.43-1.58	1.52-1.65	-6.11	2.64	12.38

Structure stability is investigated by two methods: (a) Gibbs free energy of binding (ΔG) and (b) the frequencies obtained from infrared spectra. ΔG is calculated from:

$$\Delta G = (\Delta E + \Delta ZPE - T\Delta S) / n_t \quad (1)$$

Where ΔE is the total energy difference between products and reactants, ΔZPE is the change in the zero-point energy, and n_t is the total number of atoms. The calculated Gibbs free energy in Table 1 for all the selected flakes are negative this means that the free energy of the products is less than the sum of Gibbs free energies for the stable reactants. Therefore, the investigated shBN here with edge reconstructions and modified surface by interaction with different groups and elements correspond to chemically stable systems [103]. Additionally, the free energy of shBN is comparable to that of square graphene quantum dots (SGQDs) with the same number of atoms, for example $\Delta G=-6.48$ eV for shBN-H and $\Delta G=-7.25$ eV for SGQDs-H. This free energy of binding can be further enhanced, up to $\Delta G \sim -7.1$ eV, by passivation with O atoms or in the pristine case. The significant enhancement of the binding energy in pristine flakes is a result of strong edge reconstructions as reported by F. Ersan et al. [104]. Additional demonstration of the stability is achieved by performing intrinsic reaction coordinate (IRC) calculations that provide a unique connection between the structures of the reactants and products [105, 106]. The reaction coordinate diagram, Fig. 6 (d), for shBN-COOH-Z, as illustrative example, gives optimized product structure identical to the one that we are working on. The stability can also be checked by calculating the vibrational frequencies, see Fig. 7 in Appendix B. The positive frequencies in the infrared (IR) spectra indicate that the found stationary point of the potential energy of the system is not a saddle point (i.e. no imaginary frequencies) and the functionalized shBN are geometrically stable. Our next step is to study the relaxed structure of shBN-H after adsorption of six hexahydrated metals, namely Cd, Co, Cr, Cu, Fe, and Zn. After this we select some of the resultant systems and apply chemical functionalization to see its effect on the adsorption process.

Table 2 gives the calculated adsorption distance (d_m) which is defined as the minimum distance between the adsorbed metal and the flake, and the Hirshfeld charge [107] on the hexahydrated metal ($Q=Q(\text{after adsorption}) - Q(\text{before adsorption})$). The adsorption energy (E_a) is also shown in Table 2 which is given by:

$$E_a = E_{\text{shBN-H}} + E_{\text{m.6H}_2\text{O}} - E_{\text{shBN-H-m.6H}_2\text{O}} \quad (2)$$

Where $E_{\text{shBN-H}}$, $E_{\text{m.6H}_2\text{O}}$, $E_{\text{shBN-H-m.6H}_2\text{O}}$ is the total energy of hydrogenated flake, hydrated metal, and the optimized system after adsorption, respectively. The last two columns give the energy gap (ΔE) and the total electric dipole moment (TEDM) that will be discussed in the next subsection. Fig. 2 shows the optimized structures after adsorption of selected hexahydrated metals on different positions of the quantum dots, shBN-H-Co-Z in Fig. 2 (a) represents hexahydrated Co adsorbed by shBN-H on its zigzag edge and shBN-H-Co-S (Fig. 2 (b)) represents the same adsorption on the surface, and similarly the adsorption on armchair edge (A) in Fig. 2 (c).

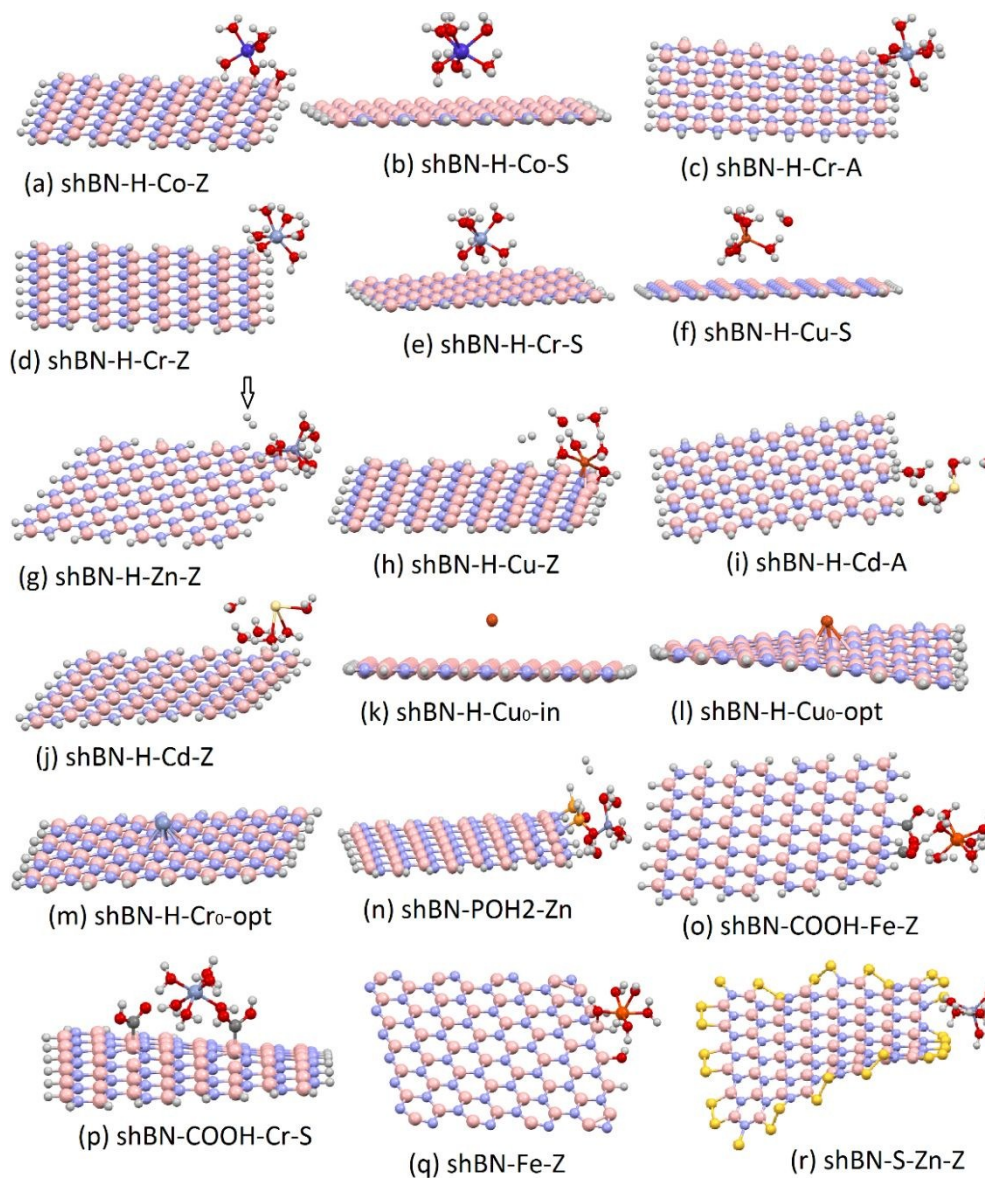


Fig. 2. Relaxed structures of shBN-H after adsorption of different hexahydrated metals.

The high adsorption distance (d_m) in Table 2 show that the hydrated metals are physically adsorbed by the hydrogenated shBN except for Cu that is chemically adsorbed on the zigzag edge. The charge-transfer to hydrated system ($Q(e)$) is a good indicator of the interaction between the adsorbing flake and the adsorbed metal where high value of Q implies high adsorption. For instance, $Q = 0.02 e$ in shBN-H-Cr-S indicates weak adsorption of hexahydrated Cr on the surface. The positive values of the adsorption energies in Table 2 and the selected infrared spectra with the positive frequencies (Fig. 7 Appendix B) confirm that the metals are successfully adsorbed and the resultant compounds are stable. Here we consider the adsorption of hydrated

metals consisting of several atoms which is important to show the nature of metals in aqueous wastewater environment. However, in this strategy it is difficult to obtain a direct relation between d_m , Q , and E_a (namely high/low d_m corresponds to low/high Q and E_a as in Cu-Z or Fe-Z in Table 2) due to the dispersion of the adsorbed atoms around the adsorption position. For instance, the adsorption energy of Cd on the zigzag edge ($E_a=4.23$ eV) is higher than its adsorption energy on armchair edge ($E_a=3.97$ eV) nevertheless the former has higher d_m than the later. This is because, as seen from Fig. 2 (i) and (j), majority of atoms in the hexahydrated system in the former case are adsorbed with smaller adsorption distance with respect to the later one, thus the average adsorption length of shBN-H-Cd-Z is smaller than that of shBN-H-Cd-A.

Table 2. d_m is the adsorption distance of the metal on the flake, Q is the Hirshfeld charge of the adsorbed metal, E_a is the adsorption energy, ΔE is the energy gap, and TEDM is the total electric dipole moment.

Structure	Adsorption, Metal-site	d_m (Å)	Q (e)	E_a (eV)	ΔE (eV)	TEDM (D)
shBN-H	Cd-A	4.98	0.18	3.97	3.65	4.48
	Cd-Z	5.37	0.15	4.23	3.43	1.71
	Cd-S	3.26	0.11	4.49	3.29	6.97
	Co-A	3.62	0.06	2.99	1.28	6.18
	Co-Z	4.04	0.39	2.87	1.62	6.38
	Co-S	3.92	0.02	2.68	1.39	7.01
	Cr-A	3.55	0.04	0.75	1.39	9.98
	Cr-Z	3.75	0.12	0.39	1.71	4.02
	Cr-S	3.99	-0.02	0.64	1.18	8.33
	Cu-A	4.18	0.05	3.18	1.34	5.55
	Cu-Z	2.08	0.63	8.83	5.44	6.46
	Cu-S	3.78	-0.02	2.95	1.23	8.15
	Fe-A	3.82	-0.01	0.47	1.26	6.59
	Fe-Z	3.91	0.05	0.20	1.34	7.45
	Fe-S	3.8	0.03	0.61	1.36	6.75
	Zn-A	3.31	0.16	7.07	5.74	12.81
Zn-Z	3.72	0.46	7.87	5.54	5.57	
Zn-S	3.96	-0.02	2.89	1.29	8.23	
shBN-COOH	Fe-A	3.66	0.16	1.63	0.88	6.41
	Fe-Z	3.52	0.23	6.07	2.58	8.01
shBN	Fe-N	3.45	0.06	1.82	-1.29	63.04
	Fe-B	2.13	0.4	1.75	0.18	64.66
shBN-O	Fe-Z	3.07	0.6	1.41	0.91	26.58
shBN-OH	Zn-Z	3.05	0.27	11.61	5.08	9.59
shBN-POH2	Zn-Z	3.66	-0.09	9.10	5.34	8.44
shBN-S	Zn-Z	3.33	1.02	8.71	0.15	25.81
	Zn-A	3.54	1.21	8.01	-0.09	50.51
shBN-COOH	Cr-S	3.42	1.09	8.65	2.11	15.49

Therefore, in order to have a clear relation between these parameters and also the metal selectivity, we study the adsorption of separate metals on the surface. As seen in Fig. 2 (j), the metal is placed 3 Å at the top of the central ring. The calculations show that Cd has the lowest adsorption strength, $E_a=0.08$ eV with $d_m=3.57$ Å and $Q=0.08$ e, followed by Zn with $E_a=1.66$ eV, $d_m=2.27$ Å and $Q=0.19$ e. The four elements, Co, Cr, Cu, and Fe, form chemical bonds ($d_m\sim 2.1$ Å) with the flake (in Fig. 2 k, l for Cu and Cr) and therefore have high adsorption energies, namely $E_a=3.6$, 2.8, 2.5, 2.2, and 1.7 eV, respectively. Thus Co is the strongly adsorbed metal by the boron nitride flake while Cd is the weakly adsorbed one. Additionally, chemical modifications can improve the adsorption process. As given in Table 2, the attachment of two COOH groups to the Z-edge of the flake (shBN-COOH-Fe-Z)

increases the adsorption energy from $E_a = 0.2$ eV to 6.1 eV. In general, the adsorption strength increases by chemical functionalization in all the selected flakes.

An important phenomenon that occurs through the adsorption process is the evolution of H_2 molecules as shown in Fig. 2 (g), (h), and (n). This effect is observed only in hydrated Zn and Cu where two of the hydrating water molecules split into two OH groups (see Fig. 2 (h)) and two hydrogen atoms forming H_2 molecules. Similar calculations on square graphene quantum dots (GQDs) adsorbing hydrated Zn and Cu like in Fig. 2 (g), (h) have been performed to test the H_2 evolution. We found that no water splitting occurs in case of GQDs and the optimized structure is similar to that given in Fig. (c) or (d) which confirm that the H_2 evolution is related to only shBN quantum dots. A future work on this phenomenon is to study the interaction of these hydrated metals with similar nitride-based materials such as GaN [108, 109]. Detailed description of the observed water splitting on the shBN-H will be presented in section 3.3.

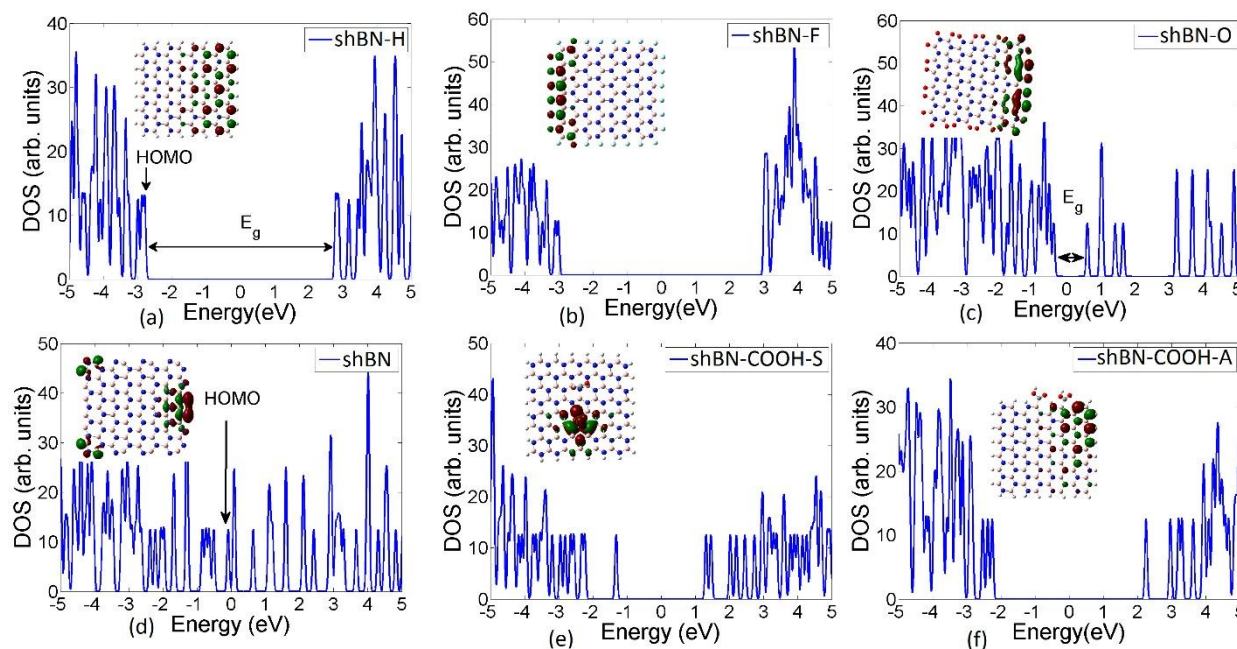


Fig. 3. Electronic density of states of shBN-H before (a) and after functionalization (b-f). The insets show the HOMO distribution.

3.2 ELECTRONIC PROPERTIES

The effect of chemical functionalization and metal adsorption on the electronic properties of shBN is clarified by studying the electronic density of states (DOS) and the spatial distribution of the highest occupied molecular orbital (HOMO). Gaussian function with broadening $\alpha \sim 0.032$ eV is used in our DOS calculations. Fig. 3 shows the DOS of nonfunctionalized flake (in Fig. 3 (a)) and the functionalized flakes in the rest parts of the figure. The calculated band gap for shBN-H ($\Delta E = 5.7$ eV) indicates that the selected flake is insulator, that gap can be tuned by attaching different elements or chemical groups. ΔE can be increased to ~ 6.1 eV by replacing H with fluorine on the edges or decreased to 0.16 eV in case of pristine flakes (Fig. 3 (d)). Intermediate values can be obtained by different functionalities such as two thionyl groups attached to surface ($\Delta E = 3.56$ eV, see Fig. 1 (f) and Table 1) and two COOH groups attached to the armchair edge ($\Delta E = 4.51$ eV, Table 1 and Fig. 3 (e)). The changes in the band gap depend on the number of electrons provided by the functionalizing element for example F gives one electron to passivate B or N edge atoms to form strong sigma bond. While passivation with COOH, O, or S provides not only one electron for passivation but also additional p electron to form weak π bonds with the flake that decrease the band gap [95,100]. To generalize our results for different sizes of the shBN-H, we study the effect of number of atoms on the electronic band gap. The calculated values of ΔE are 6.10, 5.68, 5.59, 5.50, 5.46, and 5.45 eV for $n_t = 32, 74, 132, 270, 342,$ and 456 atoms (see Fig. 6 (c) in Appendix A). The results indicate that ΔE decreases gradually by increasing the size (number of atoms) until reaching a value similar to that in the infinite hBN sheet, $\Delta E \sim 5.5$ eV [2]. Additionally, the observed significant decrease of the band gap upon modification with chemical groups or elements is also observed in larger dots with $n_t = 342$ atoms, namely the band gap, 5.46 eV, decreases to 4.57 eV when 4 COOH groups attached to the armchair edges or to 1.82 eV when attached to the surface.

The attachment position (to either N or B atoms) has an important role in controlling ΔE , where for example $\Delta E=4.51$ eV when COOH groups are attached to B atoms (shBN-COOH-A) and $\Delta E=5.64$ eV for COOH attached to N atoms (shBN-COOH-Z). As discussed above, The B-C bond length (~ 1.6 Å) is higher than the N-C (~ 1.4 Å) bond length (see Table 1). This means that the bond energy and the corresponding molecular energy in shBN-COOH-A, with C attached to B atom, is lower than that of the shBN-COOH-Z. The low energy states in the former decrease its energy gap relative to the later. In case of surface attachment, the band gap experiences additional decrease because in this case all surface atoms are already relaxed with three sigma bonds with neighbor B/N atoms and the additional bonds just contribute to the decrease of ΔE . The TEDM also depends on the attachment position, it can be seen from Table 1 that same group attachments to the armchair edge always have higher TEDM than to the zigzag edge. This is a result of the different geometrical shape that the group takes when attached to the edges where local dipoles formed between group atoms can sum up to increase the TEDM or cancel each other to decrease it. For illustration, we discuss the shBN-H before and after attachment of thionyl (SOH) groups to both the edges (A and Z). It is seen from Table 1 that the TEDM increases from 4.67 (D) in shBN-H to 12.14 (D) after attaching SOH to A-edge and decreases to 2.96 (D) when attached to Z-edge. In the first attachment the two SOH groups points toward the same direction (Fig. 1 (e)), thus local dipoles between S-O will sum up in this direction. In contrast, when attached to the Z-edge the SOH groups points in opposite directions (Fig. 1 (f)) leading to the significant decrease in the total dipole. Another interesting result is the huge TEDM=54.98 (D) obtained in pristine shBN flake due to the large edge deformation. This system is expected to have interesting adsorption and interaction properties. The adsorption process also affects the TEDM, in most cases this effect increases the total dipole, as given in Table 3, while in other cases it decreases the dipole such as the adsorption of hydrated Cd on the zigzag edge of shBN-H. The increased TEDM in the first case is obviously because of the new local dipoles from the hydrated metals that sum up, if they are in the same direction, to increase the dipole or decrease it in the second case if they point in different directions as discussed above. The TEDM depends also on the total charge on the hydrated metal (Q), the charge on the flake neighbour atoms (Q1), and the separation between them. Due to the large dispersion of the hydrated metals molecules on the flakes during the adsorption process, it is very difficult to obtain a direct relation between the charge on metals and the increase/decrease of the TEDM. However, such relation can be obtained by considering the simple case of single elements adsorption. We consider the adsorption of Co and Cd that show highest and lowest adsorption energy, respectively. The elements are situated above the center of the central ring, see Fig. 6 (e), (f). We then consider the sum of the charges on the 6 atoms of the ring (Q1) and compare the difference Q-Q1 in both metal cases. The calculations show that, the difference equals 0.317 e and 0.054 e for adsorbed Co and Cd, respectively, consequently the TEDM should be higher in the first case. Of course this is very simple method however it can provide a link between TEDM and partial charge distribution around adsorbed metals. The values of the TEDM for both the cases in Fig. 6 (e), (f) confirm the previous discussion.

Surface attachment of chemical groups can also provide a strong effect on the band gap due to the p electrons provided by the functional groups as discussed above. The HOMO distribution shown in Fig. 3 helps to understand the position of the new energy levels added by the attached elements or groups where, for instance, in Fig. 3 (e) the HOMO cubes distribute on one of the COOH groups attached on the surface implying that the HOMO originated from pi electron of C atom. While in case of shBN-H, the HOMO distribution is on the N atoms which means that it originates from the electron pair in the 2s orbital. The localized distribution of the cubs on single N atoms confirms that the electron pair is from the N atom. This distribution around N atoms significantly decreases by attaching O atoms to the edges, Fig. 3 c, as a result of the more interactive electron in 2p orbital from each O atom.

The adsorption of hydrated metals also has a significant effect on the electronic properties of the shBN-H flakes as can be seen from the DOS presented in Fig. 4. New peaks appear in the low energy region leading to decrease in the flake wide band gap to $\Delta E=3.65$ eV in shBN-H-Cd-A or to $\Delta E= 1.26$ in shBN-H-Fe-Z (see Table 2 and Fig. 4 (a), (b)). These low energy peaks represent energy levels from the adsorbed metals as seen from the corresponding HOMO distributions, their appearance as the HOMO means that they form weak bonds and can be removed without deforming the flake.

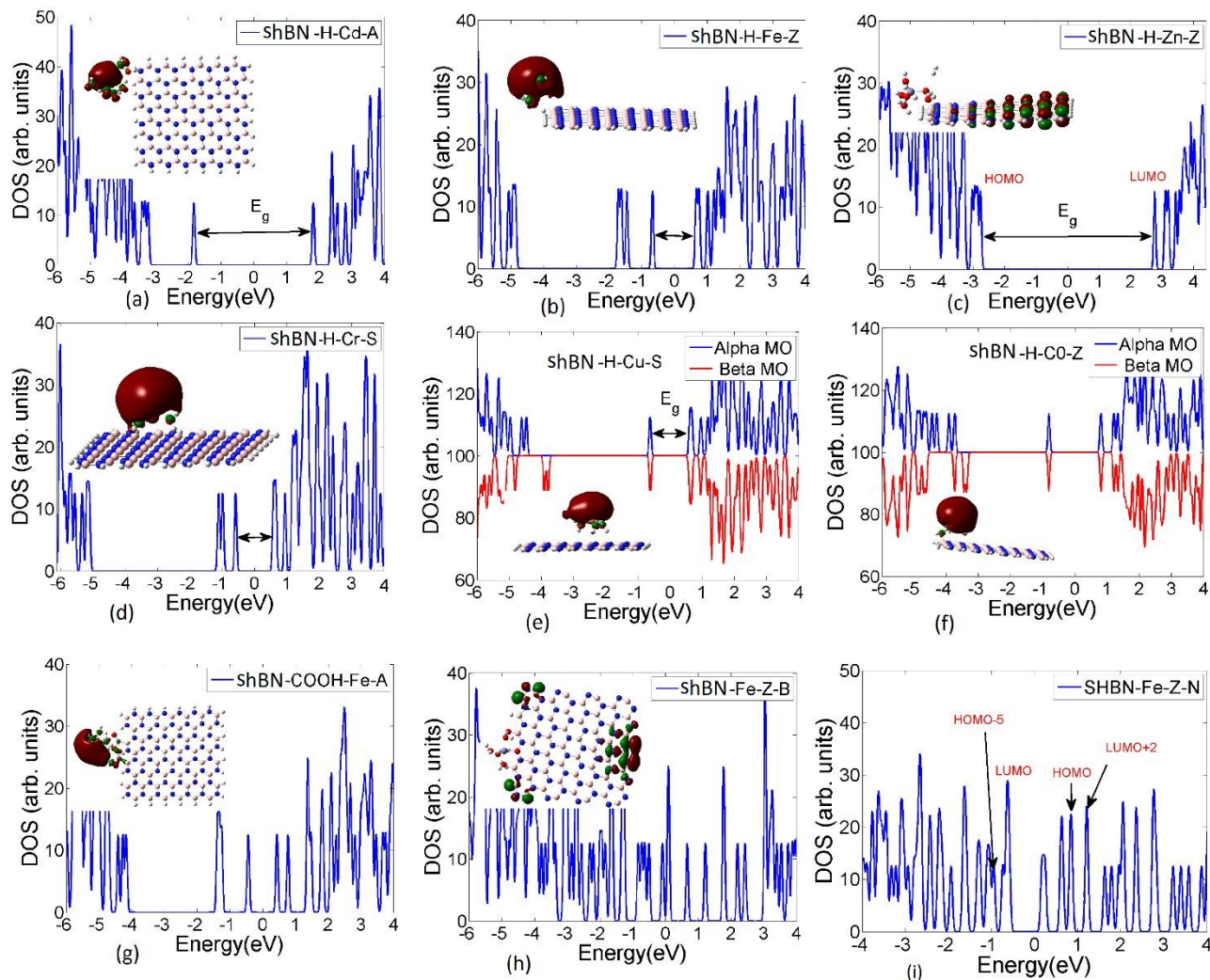


Fig. 4. DOS of shBN-H after adsorption of hydrated metals. Alpha and beta MO represent spin up and spin down MO, respectively.

It is observed from Table 2 that the adsorption of hydrated Fe and Zn on shBN and shBN-S, respectively, results in a negative energy gap due to the overlap between conduction and valence bands [110-113]. The overlap can be seen in Fig. 4 (i) where the peaks in the energy region between the HOMO-5 and HOMO+2 represent mixed molecular orbitals from HOMO-4 to LUMO+1. The origin of this transformation from the semiconductor to the semimetal is the additional electrons from the adsorbed metals that form weak bonds with the flakes. This weak bonds appear in the tiny gap region shifting the top of the valence band to higher energy than the LUMO energy. In other cases, such as adsorption of Fe by B atoms in shBN no band crossing is observed and $\Delta E=0.18$ eV. The adsorbed hydrated metal forms strong chemical bonds with B atoms, as seen in Fig. 4 (h) inset, and the corresponding molecular orbitals have energies lower than that of the HOMO. This explanation is confirmed by the distribution of HOMO, in Fig. 4 (h) inset, on the corners of the flake and not on the adsorbed metal as in Fig. 4 (i).

3.3 Water splitting

In order to have more information about how the phenomenon of water splitting occurs during the adsorption of hydrated Zn and Cu, the oxygen evolution reaction (OER) and hydrogen evolution reaction (HER) on shBN will be investigated. The adsorption of O, OH, and OOH on the edge and surface of shBN-H will be considered to determine the overpotential required for O₂ evolution. The following reaction mechanism is used to explain the OER:



Where * represent the shBN-H. The free energy (ΔG) for each step of the above four steps reaction can be calculated from the following equations:

$$\Delta G_1 = E(*\text{OH}) - E(*) - E_{\text{H}_2\text{O}} + 0.5E_{\text{H}_2} + (\Delta\text{ZPE} - T\Delta S)_1 - eU \quad (7)$$

$$\Delta G_2 = E(*\text{O}) - E(*\text{OH}) - E_{\text{H}_2\text{O}} + 0.5E_{\text{H}_2} + (\Delta\text{ZPE} - T\Delta S)_2 - eU \quad (8)$$

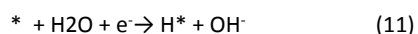
$$\Delta G_3 = E(*\text{OOH}) - E(*\text{O}) - E_{\text{H}_2\text{O}} + 0.5E_{\text{H}_2} + (\Delta\text{ZPE} - T\Delta S)_3 - eU \quad (9)$$

$$\Delta G_4 = E(*) - E(*\text{OOH}) + E_{\text{O}_2} + 0.5E_{\text{H}_2} + (\Delta\text{ZPE} - T\Delta S)_4 - eU \quad (10)$$

Where $\Delta G_{1..4}$ are the free energy steps, ΔZPE is the zero-point energy difference because of the reaction, ΔS is the change in entropy, and U is the applied potential. An ideal catalyst would need a thermodynamic potential equal to 4.92 eV for water splitting, i.e. 1.23 eV for each step. To overcome the intrinsic activation barriers of the catalyst and other barriers from the interaction medium, additional potential is required which is called overpotential [114]. Thus, the overpotential can be estimated by subtracting 1.23 eV from the maximum ΔG of these steps. The calculated ΔG values (at applied bias $U=0$ V and $T=298.15$ K) for the adsorption on the surface for the four steps are shown in the free energy diagram in Fig. 5 (g), from which the overpotential for OER on the edge and surface is $\eta=0.78$ and 0.52 V, respectively.

For OER on both the edge and the surface, the maximum free energy of the four steps is that one of the first step ($\Delta G_1=1.75$ eV for surface and $\Delta G_1=2.01$ eV for edge) thus the overpotential will be required to initiate the dissociation of H_2O on shBN-H to produce OH^* . The obtained η for OER on the surface is 0.52 V which is lower than that in several extensively used water oxidation catalysts: WO_3 (0.63 V), $\text{Bi}_4\text{NbO}_8\text{Cl}$ (0.69 V), and graphene (0.57 V) [115-117].

The HER in neutral and alkaline solutions take place using the following reaction [118]:



With H^* represent hydrogen adsorbed on the edge or the surface of shBN-H. From eqs. 11 and 12, the HER activity can be evaluated from the free energy (ΔG_{H^*}) variation due to the adsorption of H [119]. Here we calculate the HER activities for solid gas model (i.e. the effect of solvation is not considered) to decrease the computational cost. A good HER catalyst should have ΔG_{H^*} close to 0, our calculations (shown in Fig. 5 (e)) imply that shBN-H is a good HER catalyst with $\Delta G_{\text{H}^*}=0.11$ eV for adsorption on the edge. Therefore, due to the low overpotential for OER and low ΔG_{H^*} for HER, shBN quantum dots can be considered as potential catalysts for water splitting.

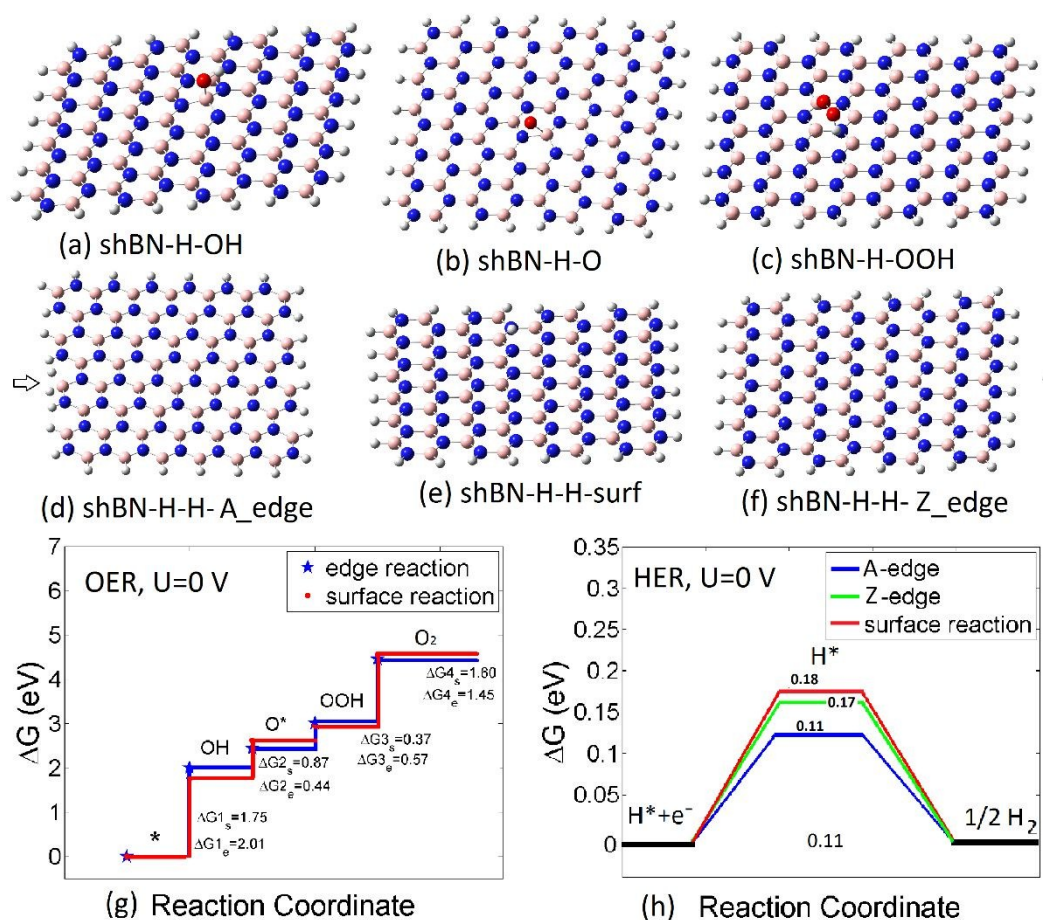


Fig. 5. Optimized structures of shBN with OH (a), O (b), and OOH (c) adsorbed on the surface, and optimized structures after adsorption of hydrogen (d-f). The free energy diagram of OER (g) and the HER (h).

4. CONCLUSION

The density functional theory calculations are employed to investigate the electronic and adsorption properties of shBN quantum dots before and after chemical functionalization with different elements and groups. The stability calculations show that all the chosen flakes are stable where the negative free energy of binding, positive adsorption energy and frequencies indicate that the resultant structures from interaction between the functionalized quantum dots and the hydrated metals are energetically stable. The structure stability and interactivity are significantly enhanced by chemical modification, for instance the free energy and total electric dipole moment can be enhanced from -6.5 eV and 4.6 D in hydrogenated flakes to -7.1 eV and 54.6 D, respectively, in pristine flakes. This effect occurs not only in pristine but also in sulfured and oxygenated flakes which in turn improves their adsorption properties. The band structures can be finely tuned by the edge passivation, where a wide band gap (~6 eV) can be obtained in fluorinated flakes and tiny gap (~0.2 eV) in sulfured ones. The hexahydrated metals, namely Co, Cr, Fe, Cu, Zn, and Cd, successfully adsorb on the surface and the edges of shBN-h. Chemical functionalization greatly enhances the adsorption capability of these flakes. For instance, the adsorption energy of Zn on the surface of hydrogenated shBN increases from 0.6 to 8.6 eV after the attachment of two COOH groups to the surface. Alongside with the successful adsorption of all the selected metals, it is also noted that hydrogen molecules evolve through the interaction with the hydrated metals, for example hydrogen molecule evolved through the adsorption of hexahydrated Zn on the flake edge. The overpotential needed to initiate OER on the surface of shBN is 0.52 V. Additionally, the calculated hydrogen adsorption strength on the edge of shBN for the HER is $\Delta G_{\text{H}^*} = 0.11$ eV. Therefore, in addition to the capability to filtering out different metals from wastewater, the low overpotential and hydrogen adsorption strength imply that boron nitride flakes are also potential candidates for efficient water splitting.

Conflicts of interest

There are no conflicts to declare.

Acknowledgements

This work is supported by Postgraduate Education Reform Project of Jiangsu Province. This collaborative research utilized Imam Abdulrahman Bin Faisal (IAU)'s Bridge HPC facility, supported by IAU Scientific and High Performance Computing Center. <https://doi.org/10.5281/zenodo.1117442>. W.O. Younis (Originally affiliated to Physics Department, Faculty of Science, Beni-Suef University, Beni-Suef City, Egypt) acknowledges the collaborated research between Beni-Suef University and IAU. VAS acknowledges funding by EU H2020 RISE project CoExAN (Grant No. H2020-644076) and support by the RCN CoE funding scheme (Grant No. 262633, "QuSpin").

APPENDIX A

The calculated band gaps using different basis sets and functionals are presented in Fig. 6 (a, b) to verify the adequacy of the results obtained from b3lyb/3-21g*. Additionally, in Fig. 6 (c), the band gaps for different total number of atoms and functionals are given to show the effect of size and the effect of functionals on large QDs. The intrinsic reaction coordinate diagram in Fig. 6 (d) for shBN-COOH-Z, as illustrative example, confirms the stability of the optimized product structures.

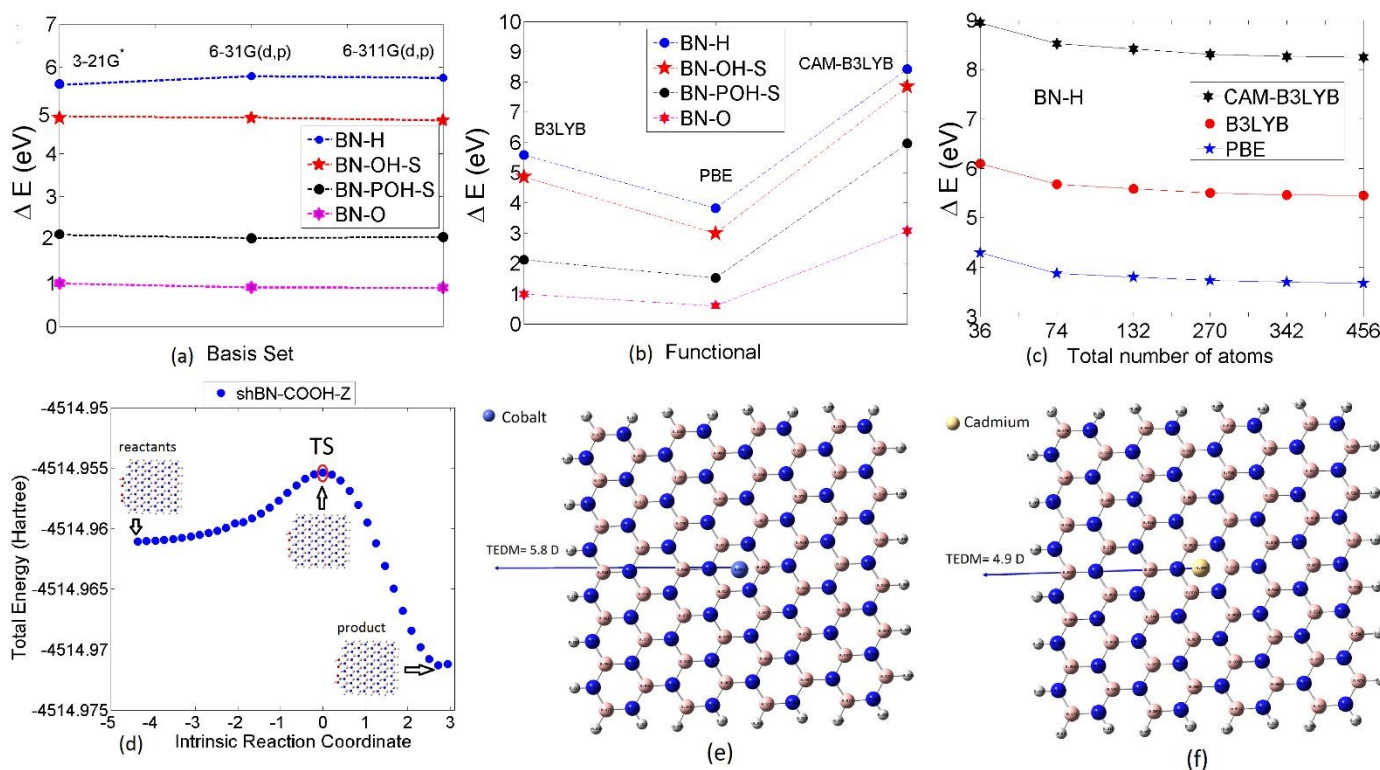


Fig. 6. (a) The obtained electronic energy gap (ΔE) using the b3lyb functional for different basis sets. (b) ΔE using 3-21g* with different functionals. (c) shBN-H band gap for different number of atoms using different functionals and 3-21g* basis set. (d) The intrinsic reaction coordinate diagram for shBN-COOH-Z. Mulliken Charges distribution and TEDM for Co (a) and Cd (f) single atoms adsorbed on the surface of shBN-H.

APPENDIX B

Fig. 7 presents the IR spectra of selected shBN flakes before/ after chemical functionalization and adsorption of hydrated metals. The structures stability is confirmed by the obtained positive frequencies for all the IR intensities.

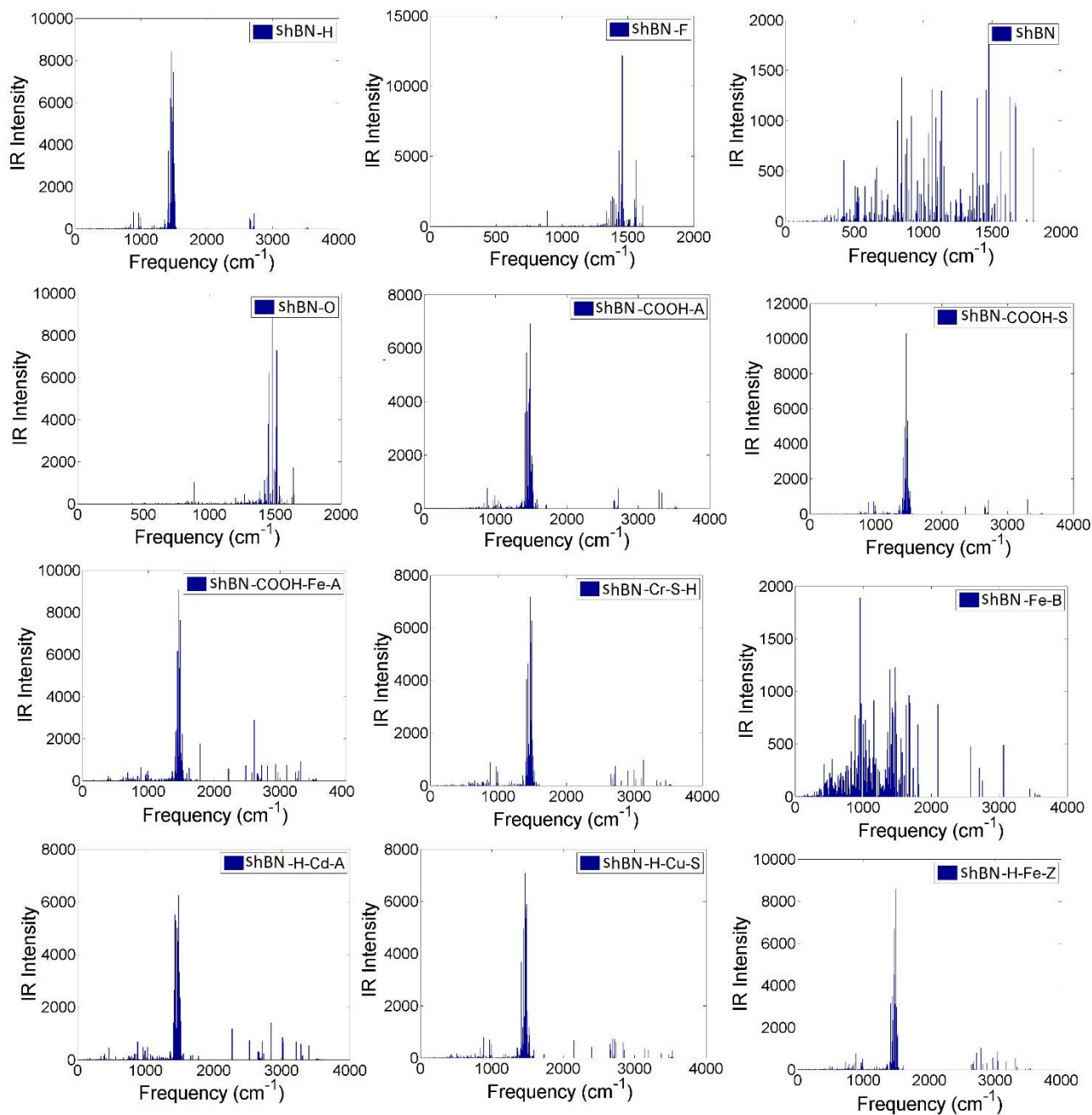


Fig. 7. Infrared spectra of selected shBN flakes.

References

- [1] A. Pakdel, Y. Bando, and D. Golberg, *Chem. Soc. Rev.*, 2014, **43**, 934.
- [2] L. Song, L. Ci, H. Lu, P. B. Sorokin, C. Jin, J. Ni, A. G. Kvashnin, D. G. Kvashnin, J. Lou, B. I. Yakobson, and P. M. Ajayan, *Nano Lett.*, 2010, **10**, 3209.

- [3] A. Nag, K. Raidongia, K. P. S. Hembram, R. Datta, U. V. Waghmare, and C. N. R. Rao, *ACS Nano*, 2010, **4**, 1539.
- [4] G. Giovannetti, P. A. Khomyakov, G. Brocks, P. J. Kelly, and J. van den Brink, *Phys. Rev. B*, 2007, **76**, 073103.
- [5] C. R. Dean, A. F. Young, I. Meric, C. Lee, L. Wang, S. Sorgenfrei, K. Watanabe, T. Taniguchi, P. Kim, K. L. Shepard, and J. Hone, *Nat. Nanotechnol.*, 2010, **5**, 722.
- [6] W. Yang, G. Chen, Z. Shi, C.-C. Liu, L. Zhang, G. Xie, M. Cheng, D. Wang, R. Yang, D. Shi, K. Watanabe, T. Taniguchi, Y. Yao, Y. Zhang, and G. Zhang, *Nat. Mater.*, 2013, **12**, 792.
- [7] M. Toth and I. Aharonovich, *Annu. Rev. Phys. Chem.*, 2019, **70**, 123.
- [8] X. Liu and M. C. Hersam, *Nat. Rev. Mater.*, 2018, **30**, 1801586 .
- [9] S. Kim, J. E. Fröch, J. Christian, M. Straw, J. Bishop, D. Totonjian, K. Watanabe, T. Taniguchi, M. Toth, and I. Aharonovich, *Nat. Commun.*, 2018, **9**, 2623.
- [10] J. E. Fröch, Y. Hwang, S. Kim, I. Aharonovich, and M. Toth, *Adv. Opt. Mater.*, 2019, **7**, 1801344.
- [11] J. D. Caldwell, A. V. Kretinin, Y. Chen, V. Giannini, M. M. Fogler, Y. Francescato, C. T. Ellis, J. G. Tischler, C. R. Woods, A. J. Giles, M. Hong, K. Watanabe, T. Taniguchi, S. A. Maier, and K. S. Novoselov, *Nat. Commun.*, 2014, **5**, 5221.
- [12] S. Dai, Z. Fei, Q. Ma, A. S. Rodin, M. Wagner, A. S. McLeod, M. K. Liu, W. Gannett, W. Regan, K. Watanabe, T. Taniguchi, M. Thiemens, G. Dominguez, A. H. C. Neto, A. Zettl, F. Keilmann, P. Jarillo-Herrero, M. M. Fogler, and D. N. Basov, *Science (80-.)*, 2014, **343**, 1125.
- [13] D. N. Basov, M. M. Fogler, and F. J. Garcia de Abajo, *Science (80-.)*, 2016, **354**, aag1992.
- [14] A. J. Giles, S. Dai, I. Vurgaftman, T. Hoffman, S. Liu, L. Lindsay, C. T. Ellis, N. Assefa, I. Chatzakis, T. L. Reinecke, J. G. Tischler, M. M. Fogler, J. H. Edgar, D. N. Basov, and J. D. Caldwell, *Nat. Mater.*, 2018, **17**, 134.
- [15] M. Tamagnone, A. Ambrosio, K. Chaudhary, L. A. Jauregui, P. Kim, W. L. Wilson, and F. Capasso, *Sci. Adv.*, 2018, **4**, eaat7189.
- [16] N. G. Chopra, R. J. Luyken, K. Cherrey, V. H. Crespi, M. L. Cohen, S. G. Louie, and A. Zettl, *Science (80-.)*, 1995, **269**, 966.
- [17] D. Golberg, Y. Bando, C. C. Tang, and C. Y. Zhi, *Adv. Mater.*, 2007, **19**, 2413.
- [18] Z. Chen, J. Zou, G. Liu, F. Li, Y. Wang, L. Wang, X. Yuan, T. Sekiguchi, H. Cheng, and G. Q. Lu, *ACS Nano*, 2008, **2**, 2183.
- [19] H. Zeng, C. Zhi, Z. Zhang, X. Wei, X. Wang, W. Guo, Y. Bando, and D. Golberg, *Nano Lett.*, 2010, **10**, 5049.
- [20] K. J. Erickson, A. L. Gibb, A. Sinitskii, M. Rouseas, N. Alem, J. M. Tour, and A. K. Zettl, *Nano Lett.*, 2011, **11**, 3221.
- [21] L. Li, L. H. Li, Y. Chen, X. J. Dai, P. R. Lamb, B.-M. Cheng, M.-Y. Lin, and X. Liu, *Angew. Chemie Int. Ed.*, 2013, **52**, 4212.
- [22] S. Zhang, G. Lian, H. Si, J. Wang, X. Zhang, Q. Wang, and D. Cui, *J. Mater. Chem. A*, 2013, **1**, 5105.
- [23] L. Lin, Y. Xu, S. Zhang, I. M. Ross, A. C. M. Ong, and D. A. Allwood, *Small*, 2014, **10**, 60.
- [24] H. Li, R. Y. Tay, S. H. Tsang, X. Zhen, and E. H. T. Teo, *Small*, 2015, **11**, 6491.
- [25] Z. Lei, S. Xu, J. Wan, and P. Wu, *Nanoscale*, 2015, **7**, 18902.
- [26] P. Thangasamy, M. Santhanam, and M. Sathish, *ACS Appl. Mater. Interfaces*, 2016, **8**, 18647.
- [27] B. Liu, S. Yan, Z. Song, M. Liu, X. Ji, W. Yang, and J. Liu, *Chem. - A Eur. J.*, 2016, **22**, 18899.
- [28] B. Huo, B. Liu, T. Chen, L. Cui, G. Xu, M. Liu, and J. Liu, *Langmuir*, 2017, **33**, 10673.
- [29] D. Peng, L. Zhang, F.-F. Li, W.-R. Cui, R.-P. Liang, and J.-D. Qiu, *ACS Appl. Mater. Interfaces*, 2018, **10**, 7315.
- [30] S. Tang, H. Wang, Y. Zhang, A. Li, H. Xie, X. Liu, L. Liu, T. Li, F. Huang, X. Xie, and M. Jiang, *Sci. Rep.*, 2013, **3**, 2666.
- [31] A. Mishchenko, J. S. Tu, Y. Cao, R. V. Gorbachev, J. R. Wallbank, M. T. Greenaway, V. E. Morozov, S. V. Morozov, M. J. Zhu, S. L. Wong, F. Withers, C. R. Woods, Y.-J. Kim, K. Watanabe, T. Taniguchi, E. E. Vdovin, O. Makarovskiy, T. M.

- Fromhold, V. I. Fal'ko, A. K. Geim, L. Eaves, and K. S. Novoselov, *Nat. Nanotechnol.*, 2014, **9**, 808.
- [32] N. Mishra, V. Miseikis, D. Convertino, M. Gemmi, V. Piazza, and C. Coletti, *Carbon N. Y.*, 2016, **96**, 497.
- [33] L. Chen, L. He, H. S. Wang, H. Wang, S. Tang, C. Cong, H. Xie, L. Li, H. Xia, T. Li, T. Wu, D. Zhang, L. Deng, T. Yu, X. Xie, and M. Jiang, *Nat. Commun.*, 2017, **8**, 14703.
- [34] L. Chen, H. Wang, S. Tang, L. He, H. S. Wang, X. Wang, H. Xie, T. Wu, H. Xia, T. Li, and X. Xie, *Nanoscale*, 2017, **9**, 11475.
- [35] H. Arjmandi-Tash, D. Kalita, Z. Han, R. Othmen, G. Nayak, C. Berne, J. Landers, K. Watanabe, T. Taniguchi, L. Marty, J. Coraux, N. Bendiab, and V. Bouchiat, *J. Phys. Mater.*, 2018, **1**, 015003.
- [36] D. Chen, R. Qiao, X. Xu, W. Dong, L. Wang, R. Ma, C. Liu, Z. Zhang, M. Wu, L. Liu, L. Bao, H.-T. Wang, P. Gao, K. Liu, and D. Yu, *Nanoscale*, 2019, **11**, 4226.
- [37] A. Rubio, J. L. Corkill, and M. L. Cohen, *Phys. Rev. B*, 1994, **49**, 5081.
- [38] X. Blase, A. Rubio, S. G. Louie, and M. L. Cohen, *Epl*, 1994, **28**, 335.
- [39] L. A. Chernozatonskii, Y. K. Shimkus, and I. V. Stankevich, *Phys. Lett. A*, 1998, **240**, 105.
- [40] K. H. Khoo, M. S. C. Mazzoni, and S. G. Louie, *Phys. Rev. B - Condens. Matter Mater. Phys.*, 2004, **69**, 1.
- [41] S.-H. Jhi, D. J. Roundy, S. G. Louie, and M. L. Cohen, *Solid State Commun.*, 2005, **134**, 397.
- [42] C.-H. Park, C. D. Spataru, and S. G. Louie, *Phys. Rev. Lett.*, 2006, **96**, 126105.
- [43] L. Wirtz, A. Marini, and A. Rubio, *Phys. Rev. Lett.*, 2006, **96**, 126104.
- [44] W.-Q. Han, H.-G. Yu, C. Zhi, J. Wang, Z. Liu, T. Sekiguchi, and Y. Bando, *Nano Lett.*, 2008, **8**, 491.
- [45] J. Song, H. Liu, and W. Shen, *Eur. Phys. J. D*, 2018, **72**, 170.
- [46] R. B. Payod and V. A. Saroka, *Semiconductors*, 2019, **53**, 63.
- [47] C.-H. Park and S. G. Louie, *Nano Lett.*, 2008, **8**, 2200.
- [48] V. Barone and J. E. Peralta, *Nano Lett.*, 2008, **8**, 2210.
- [49] Z. Zhang and W. Guo, *Phys. Rev. B - Condens. Matter Mater. Phys.*, 2008, **77**, 1.
- [50] K. Zhao, M. Zhao, Z. Wang, and Y. Fan, *Phys. E Low-Dimensional Syst. Nanostructures*, 2010, **43**, 440.
- [51] F.-L. Shyu, *Phys. B Condens. Matter*, 2014, **452**, 7.
- [52] L. L. Li, X. F. Yu, X. J. Yang, X. H. Zhang, X. W. Xu, P. Jin, J. L. Zhao, X. X. Wang, and C. C. Tang, *J. Alloys Compd.*, 2015, **649**, 1130.
- [53] G. Seol and J. Guo, *Appl. Phys. Lett.*, 2011, **98**, 143107.
- [54] J. Li and V. B. Shenoy, *Appl. Phys. Lett.*, 2011, **98**, 013105.
- [55] X. F. Chen, J. S. Lian, and Q. Jiang, *Phys. Rev. B*, 2012, **86**, 125437.
- [56] F. Ersan, G. Gökoğlu, E. Aktürk, *Appl. Surf. Sci.*, 2014, 303, 306.
- [57] V.-T. Tran, J. Saint-Martin, and P. Dollfus, *Appl. Phys. Lett.*, 2014, **105**, 073114.
- [58] J. Ouyang, M. Long, D. Zhang, X. Zhang, J. He, and Y. Gao, *Comput. Condens. Matter*, 2015, **4**, 40.
- [59] L. A. Chernozatonskii, V. A. Demin, and A. A. Artyukh, *JETP Lett.*, 2016, **104**, 43.
- [60] L. A. Chernozatonskii, V. A. Demin, and S. Bellucci, *Sci. Rep.*, 2016, **6**, 38029.
- [61] M. Ezawa, *Phys. Rev. B*, 2007, **76**, 245415.
- [62] Z. Z. Zhang, K. Chang, and F. M. Peeters, *Phys. Rev. B*, 2008, **77**, 235411.

- [63] H. Abdelsalam, M. H. Talaat, I. Lukyanchuk, M. E. Portnoi, and V. A. Saroka, *J. Appl. Phys.*, 2016, **120**, 014304.
- [64] D. R. da Costa, M. Zarenia, A. Chaves, G. A. Farias, and F. M. Peeters, *Phys. Rev. B*, 2016, **93**, 085401.
- [65] V. A. Saroka, I. Lukyanchuk, M. E. Portnoi, and H. Abdelsalam, *Phys. Rev. B*, 2017, **96**, 085436.
- [66] L. L. Li, D. Moldovan, W. Xu, and F. M. Peeters, *Phys. Rev. B*, 2017, **96**, 155425.
- [67] H. Abdelsalam, V. A. Saroka, I. Lukyanchuk, and M. E. Portnoi, *J. Appl. Phys.*, 2018, **124**, 124303.
- [68] H. Abdelsalam, V. A. Saroka, M. Ali, N. H. Teleb, H. Elhaes, and M. A. Ibrahim, *Phys. E Low-Dimensional Syst. Nanostructures*, 2019, **108**, 339.
- [69] H. Abdelsalam, V. A. Saroka, and W. O. Younis, *Phys. E Low-Dimensional Syst. Nanostructures*, 2019, **107**, 105.
- [70] M. Zarenia, A. Chaves, G. A. Farias, and F. M. Peeters, *Phys. Rev. B*, 2011, **84**, 245403.
- [71] M. Grujic, M. Zarenia, A. Chaves, M. Tadic, G. A. Farias, and F. M. Peeters, *Phys. Rev. B*, 2011, **84**, 205441.
- [72] M. Zarenia, B. Partoens, T. Chakraborty, and F. M. Peeters, *Phys. Rev. B*, 2013, **88**, 245432.
- [73] K. Kikutake, M. Ezawa, and N. Nagaosa, *Phys. Rev. B*, 2013, **88**, 115432.
- [74] D. R. da Costa, M. Zarenia, A. Chaves, G. A. Farias, and F. M. Peeters, *Carbon N. Y.*, 2014, **78**, 392.
- [75] R. Zhang, X. Y. Zhou, D. Zhang, W. K. Lou, F. Zhai, and K. Chang, *2D Mater.*, 2015, **2**, 045012.
- [76] D. R. da Costa, M. Zarenia, A. Chaves, G. A. Farias, and F. M. Peeters, *Phys. Rev. B*, 2015, **92**, 115437.
- [77] S. Pavlović and F. M. Peeters, *Phys. Rev. B*, 2015, **91**, 155410.
- [78] Y. Liu, S. Bhowmick, and B. I. Yakobson, *Nano Lett.*, 2011, **11**, 3113.
- [79] J. Zhang, W. Zhao, and J. Zhu, *Nanoscale*, 2018, **10**, 17683.
- [80] A. Du, Y. Chen, Z. Zhu, R. Amal, G. Q. (Max) Lu, and S. C. Smith, *J. Am. Chem. Soc.*, 2009, **131**, 17354.
- [81] Y. Xi, M. Zhao, X. Wang, S. Li, X. He, Z. Wang, and H. Bu, *J. Phys. Chem. C*, 2011, **115**, 17743.
- [82] P. Xu, S. S. Yu, and L. Qiao, *Mol. Simul.*, 2013, **39**, 487.
- [83] Y. Xi, X. Zhao, A. Wang, X. Wang, H. Bu, and M. Zhao, *Phys. E Low-Dimensional Syst. Nanostructures*, 2013, **49**, 52.
- [84] S. S. Yamijala, A. Bandyopadhyay, and S. K. Pati, *J. Phys. Chem. C*, 2013, **117**, 23295.
- [85] S. S. R. K. C. Yamijala, A. Bandyopadhyay, and S. K. Pati, *Chem. Phys. Lett.*, 2014, **603**, 28.
- [86] C. Pan, M. Long, and J. He, *Results Phys.*, 2017, **7**, 1487.
- [87] M. Neek-Amal, J. Beheshtian, A. Sadeghi, K. H. Michel, and F. M. Peeters, *J. Phys. Chem. C*, 2013, **117**, 13261.
- [88] A. Bandyopadhyay, S. S. R. K. C. Yamijala, and S. K. Pati, *Phys. Chem. Chem. Phys.*, 2013, **15**, 13881.
- [89] D. Chakraborty and P. K. Chattaraj, *J. Phys. Chem. C*, 2016, **120**, 27782.
- [90] D. Chakraborty and P. K. Chattaraj, *J. Phys. Condens. Matter*, 2017, **29**, 425201.
- [91] D. Krepel, L. Kalikhman-Razvozov, and O. Hod, *J. Phys. Chem. C*, 2014, **118**, 21110.
- [92] Y. Xue, P. Dai, X. Jiang, X. Wang, C. Zhang, D. Tang, Q. Weng, X. Wang, A. Pakdel, C. Tang, Y. Bando, and D. Golberg, *J. Mater. Chem. A*, 2016, **4**, 1469.
- [93] M.J. Frisch, G.W. Trucks, H.B. Schlegel, G.E. Scuseria, et al., *Gaussian 16, Revision B.01*, Gaussian, Inc., Wallingford, CT, 2016.
- [94] K. D. Dobbs and W. J. Hehre, *J. Comput. Chem.*, 1987, **8**, 880.

- [95] H. Abdelsalam, H. Elhaes and M. A. Ibrahim, *Physica B*, 2018, **15**, 77.
- [96] H. Zheng and W. Duley, *Phys. Rev B*, 2008, **78**, 045421.
- [97] A. D. Becke, *J. Chem. Phys.*, 1993, **98**, 5648.
- [98] C. Lee, W. Yang, P.G. Parr, *Phys. Rev. B*, 1998, **37**, 785.
- [99] E. Zahedi, A. Pangh, H. Ghorbanpour, *Surf. Rev. Lett.*, 2015, **22**, 1550005.
- [100] S.K. Singh, M. Neek-Amal, F.M. Peeters, *J. Chem. Phys.*, 2014, **140**, 074304.
- [101] H. Abdelsalam, H. Elhaes, M. A. Ibrahim, *Chem. Phys. Lett.*, 2018, **696**, 138.
- [102] J. Wang, F. Ma, M. Sun, *RSC Adv.*, 2017, **7**, 16801.
- [103] R. B. Wexler, J. M. P. Martirez, A. M. Rappe, *Chem. Mater.*, 2016, **28**, 5365.
- [104] F. Ersan, O. Ü. Aktürk, E. Aktürk, S. Ciraci, *J. Phys. Chem. C*, 2018, **122**, 14598–14605.
- [105] K. Fukui, *Acc. Chem. Res.*, 1981, **14**, 12, 363.
- [106] S. Maeda, Y. Harabuchi, Y. Ono, T. Taketsugu, K. Morokuma. *Int. J. Quantum Chem.*, 2015, **115**, 258.
- [107] F.L. Hirshfeld, *Theor. Chim. Acta*, 1977, **44**, 129.
- [108] G. R. Bhimanapati, Z. Lin, V. Meunier, et al., *ACS Nano* 2015, **9**, 12, 11509.
- [109] D. Kecik, A. Onen, M. Konuk, et. al, *Appl. Phys. Rev.*, 2018, **5**, 011105.
- [110] T.D. Veal, I. Mahboob, C.F. McConville, *Phys. Rev. Lett.*, 2004, **92**, 136801.
- [111] N. Malkova, G. W. Bryant, *Phys. Rev. B*, 2010, **82**, 155314.
- [112] N. Malkoval, G. W. Bryant, *Physica B.*, 2013, **410**, 147.
- [113] A. M. Kadykov, S. S. Krishtopenko, B. Jouault, et al., *Phys. Rev. Lett.*, 2018, **120**, 086401.
- [114] X. Zou, Y. Zhang, *Chem. Soc. Rev.*, 2015, **44**, 5148.
- [115] R. Kishorea, X. Caob, X. Zhanga, A. Bieberle-Hütter, *Catal. Today*, 2019 **321–322**, 94.
- [116] X. Zhou, H. Dong, *J. Phys. Chem. C* 2017, **121**, 38, 20662.
- [117] G. Gao, S. Bottle, A. Du, *Catal. Sci. Technol.*, 2018, **8**, 996.
- [118] R. Wüthrich, J. D. Abou Ziki (2015), *Micromachining Using Electrochemical Discharge Phenomenon (Second Edition)* - Chapter 3, <https://doi.org/10.1016/B978-0-323-24142-7.00003-2>.
- [119] G. Gao, Y. Jiao, F. Ma, Y. Jiao, E. Waclawik and A. Du, *J. Phys. Chem. C*, 2015, **119**, 13124.